Effect of hydrogen passivation on luminescence-center-mediated Er excitation in Si-rich SiO_2 with and without Si nanocrystals

Oleksandr Savchyn* and Pieter G. Kik†
CREOL, The College of Optics and Photonics, University of Central Florida, 4000 Central Florida Boulevard, Orlando, Florida 32816, USA

Ravi M. Todi‡ and Kevin R. Coffey†,‡,§
Advanced Materials Processing and Analysis Center (AMPAC), University of Central Florida, 4000 Central Florida Boulevard, Orlando, Florida 32816, USA

(Received 16 January 2008; revised manuscript received 2 May 2008; published 30 May 2008)

The influence of hydrogen passivation on luminescence-center-mediated excitation of Er^{3+} in Er-doped Si-rich SiO_2 films with significantly different microstructures is studied. Photoluminescence measurements are presented for samples containing no detectable silicon nanocrystals (annealed at 600 °C) and for samples containing silicon nanocrystals (annealed at 1100 °C) as a function of hydrogen passivation temperature. Passivation is found to have little effect on the Er^{3+} photoluminescence intensity at 1535 nm in the samples that do not contain nanocrystals. In contrast, a pronounced increase in the Er^{3+} photoluminescence intensity is observed in the samples containing Si nanocrystals, which is accompanied by a similar increase in the nanocrystal photoluminescence intensity and a gradual increase in the Si nanocrystal emission lifetime. This observation is attributed to two interrelated effects, namely, (a) an increase in the density of fully passivated optically active nanocrystals due to the passivation-induced removal of silicon dangling bonds and (b) a concurrent reduction in nonradiative Er^{3+} relaxation from levels above the $^4I_{13/2}$ level due to a direct interaction of excited Er^{3+} ions with silicon dangling bonds. In addition, the observed counterintuitive gradual increase in the nanocrystal photoluminescence decay time upon passivation is successfully explained taking into account a passivation-induced change in the concentration of optically active nanocrystals with different sizes and the inhomogeneous nature of the nanocrystal-related emission band. It is shown that the combination of luminescence-center-mediated Er^{3+} excitation and silicon-dangling-bond-induced Er^{3+} de-excitation can explain at least 14 experimental observations reported by independent authors.

DOI: 10.1103/PhysRevB.77.205438 PACS number(s): 78.67.Bf, 71.35.Gg, 71.55.−i, 76.30.Kg

I. INTRODUCTION

The recent observation of luminescence-center-mediated Er^{3+} excitation in Si-rich SiO_2 [1] could provide new opportunities in silicon photonics. Erbium-doped silica has long been considered as one of the possible candidates to provide a silicon compatible light source, which is currently one of the most challenging optical components to be realized.[2–7] In its ionized state (Er^{3+}), erbium has a weakly allowed optical transition at 1.5 μm, corresponding to the transition from the first excited state ($^4I_{13/2}$) to the ground state ($^4I_{15/2}$). The first excited state typically has a lifetime in the millisecond range,[8] which provides the possibility of using it as a metastable level of a laser system. Er-based lasers have been developed using optical pumping into the $^4I_{11/2}$ and $^4I_{13/2}$ levels. These systems require laser-based pumping due to the narrow Er^{3+} absorption lines with low ($\sim 10^{-20}$–10^{-21} cm^2) absorption cross sections.[9] The Er^{3+} excitation process may be facilitated by the incorporation of sensitizers with a large absorption cross section and a high energy transfer efficiency.[10] An approach that has received a lot of attention involves the use of silicon nanocrystals incorporated into the Er-doped SiO_2 matrix.[11–18] Such composite systems can provide effective Er^{3+} excitation cross sections in excess of 10^{-16} cm^2 but also introduce significant confined-carrier optical absorption due to the existence of long-lived exciton states in the Si nanocrystals.[7,19–21] Recent research conducted on the nanocrystal-erbium interaction has suggested the presence of two different excitation mechanisms of Er^{3+} sensitization in silicon-nanocrystal-doped SiO_2 films: one involving a fast energy transfer (transfer time of <100 ns) and one involving a relatively slow energy transfer (transfer time of $\sim 1-70$ μs).[22] The presence of two types of excitation time scales has been attributed either to a nanocrystal-Er^{3+} distance-dependent transfer rate[23] or alternatively to the fast excitation of Er^{3+} by hot electrons generated in Si nanocrystals followed by a relatively slow Er^{3+} excitation via thermalized excitons in Si nanocrystals.[24] Recently, we showed[1] that Si nanocrystals (NCs) in fact only provide a small part of the Er^{3+} sensitization, while most of the Er^{3+} excitation occurs through excess-silicon-related luminescence centers in the oxide. The luminescence centers (LCs) appear to exhibit a high ($\sim 90\%$) transfer efficiency to Er^{3+} ions and to dramatically increase the effective Er^{3+} absorption cross section.[1] These observations suggest the possibility of engineering greatly enhanced Er^{3+} excitation cross sections but without the introduction of nanocrystal-induced confined-carrier absorption.

While our previous study[1] showed that only an insignificant fraction of the Er^{3+} ions is sensitized by nanocrystals, other authors observed a clear correlation between the nanocrystal and erbium emission intensities in passivation studies,[25] which suggests that a physical link does exist between the NCs and Er^{3+} optical properties. In order to inves-

tigate the role of Si nanocrystals in LC-mediated Er^{3+} excitation, here we study the effect of hydrogen passivation on the LC-Er^{3+} interaction. Hydrogen passivation has been shown to significantly improve the optical properties of the nanocrystal emission in Si-rich SiO_2 films.[25–30] The improvement is mostly due to the passivation of silicon dangling bonds (commonly referred to as P_b centers) that act as efficient exciton traps with capture times of <0.1 ns.[31,32] Silicon dangling bonds are created at the interface between the amorphous silica host and a silicon nanocrystal due to the lattice mismatch between the two materials.[33–36] Annealing a Si-nanocrystal-doped silica film in a hydrogen-rich environment results in the saturation of the dangling bonds with atomic hydrogen. This decreases the concentration of the P_b centers[25,33,37] and consequently increases the density of optically active nanocrystals in the silica host.[27,30] In addition, passivation has been observed to increase the decay time of the nanocrystal-related band.[27] The latter observation is a counterintuitive result since it is generally believed that the presence of a single dangling bond renders a nanocrystal optically "dark" due to the fast exciton capture time by dangling bonds.[31,32]

The current paper addresses the effect of hydrogen passivation on the photoluminescence of Si nanocrystals, luminescence centers, and erbium. The studies are conducted on two structurally different Er-doped Si-rich SiO_2 films: films without any detectable silicon nanocrystals and films containing Si nanocrystals. Through an investigation of the passivation-temperature-dependent optical properties of these samples, a model is developed that resolves both the unexplained correlation between the nanocrystal and erbium emission intensities and the unexpected gradual increase in the nanocrystal photoluminescence decay time upon passivation. The proposed model at once accounts for at least 14 experimental observations presented in independent studies by different scientific groups.

II. EXPERIMENTAL TECHNIQUES

A silicon- and erbium-doped SiO_2 layer was deposited onto a P-doped (100) Czochralski grown silicon wafer (resistivity of $3-7\ \Omega$ cm) by magnetron cosputtering from Si, SiO_2, and SiO_2:Er_2O_3 targets in a multigun sputtering system (AJA International, Inc., ATC-2200V). The composition and thickness of the as-deposited film was verified by Rutherford backscattering spectrometry (RBS) (General IONIX 1.7 MU Tandetron) in conjunction with the RUMP software package[38] used to fit the RBS spectra. The 110 nm thick film was found to contain 12 at. % of excess Si and 0.63 at. % of Er. A low concentration of Ar ($\sim$0.4 at. %) was also present as a result of the sputtering process. The samples were annealed for 100 s in flowing N_2 [flow rate of 3 SLPM (standard liters per minute at STP)] at ambient pressure using a rapid thermal processor (Modular Process Technology Corp., RTP-600S). For this study, two different annealing temperatures were used: one set of samples labeled LTA ("low-temperature anneal") was annealed at 600 °C, while another set of samples labeled HTA ("high-temperature anneal") was annealed at 1100 °C. As demonstrated in Ref. 1, annealing at temperatures above 1000 °C results in the formation of silicon nanocrystals, while annealing at a temperature of 600 °C does not produce silicon aggregates detectable by transmission electron microscopy. The samples were subsequently passivated for 30 min in flowing forming gas [N_2:H_2=95%:5%, flow rate of 65 SCCM (standard cubic centimeters per minute at STP)] in a tube furnace (Lindberg, 58114) at temperatures in the range of 300–600 °C and 300–800 °C for the LTA and HTA samples, respectively. The samples were allowed to cool down to room temperature in the cold zone of the furnace under a continued forming gas flow for 10 min. Unpassivated reference samples were included in all measurements, and the results have been added to the corresponding graphs at a passivation temperature of 20 °C. Photoluminescence measurements were taken at room temperature using the 351 nm emission line of a Kr-ion laser (Spectra-Physics, BeamLok 2060) as the excitation source. The pump power used was 1.32 mW and the spot size on the sample was $\sim$0.5 mm^2 in all the measurements. A single monochromator (Acton, SpectraPro 2300i) was used to disperse the collected signal, and a long pass filter (cutoff wavelength of 400 nm) was placed in front of the entrance slits to remove any collected laser signal. A thermoelectrically cooled charge-coupled device camera (Andor, DU401-BR-DD) was used to record the spectra in the visible region. A liquid-nitrogen-cooled Ge detector (Applied Detector Corp., 403S) in combination with standard lock-in techniques was used for spectral measurements in the near-infrared region. The obtained spectra were corrected for the system response. The time dependence of the photoluminescence intensity was measured by modulating the pump beam using an acousto-optic modulator (NEOS Technologies, 38210–6AS). Photoluminescence traces at 800, 900, and 1535 nm were obtained, respectively, using an avalanche photodiode (PerkinElmer SPCM-AQR), a visible–near-infrared photomultiplier tube (Hamamatsu R4330-02), and a near-infrared photomultiplier tube (Hamamatsu 5509-73), in combination with a multichannel scaler (Stanford Research Systems, SR430). The spectral resolution in all photoluminescence measurements was $\sim$15 nm. The time resolution in all measurements presented in this study was better than 80 ns.

III. RESULTS AND DISCUSSION

A. Experimental results

Figure 1 shows the measured photoluminescence (PL) spectra in the visible–near-infrared region of the LTA samples passivated at temperatures in the range of 300–600 °C. The spectrum of the unpassivated sample is included as a reference. Note that all PL spectra in this study are displayed on a logarithmic scale set to the same dynamic range (4 orders of magnitude) to facilitate comparison of the relative intensity changes upon passivation. The PL spectra in Fig. 1 show two distinct bands that are present at all passivation temperatures: a broad emission band peaking at around 550 nm and a relatively sharp emission band peaking at 981 nm. The broad emission band is characterized by a resolution-limited decay time τ ($\tau<80$ ns at $\lambda=550$ nm)

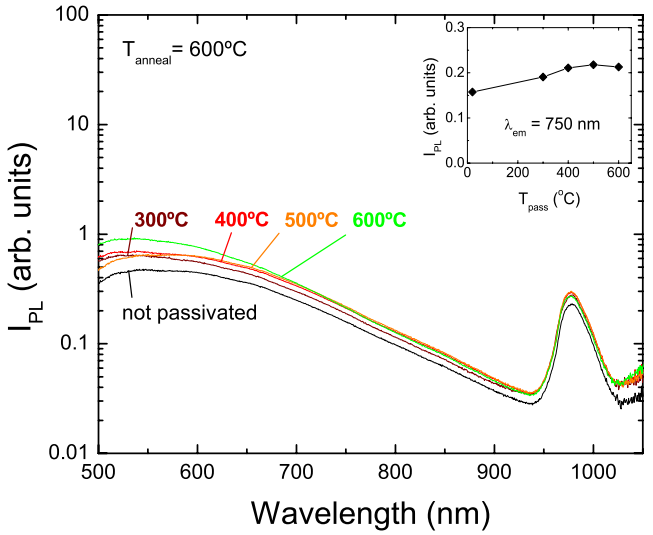

FIG. 1. (Color online) Photoluminescence spectra in the visible–near-infrared region of the LTA samples passivated in the temperature range 300–600 °C. The PL spectrum of an unpassivated sample is included as a reference. Inset: PL intensity of the luminescence center emission of the LTA samples at 750 nm as a function of passivation temperature.

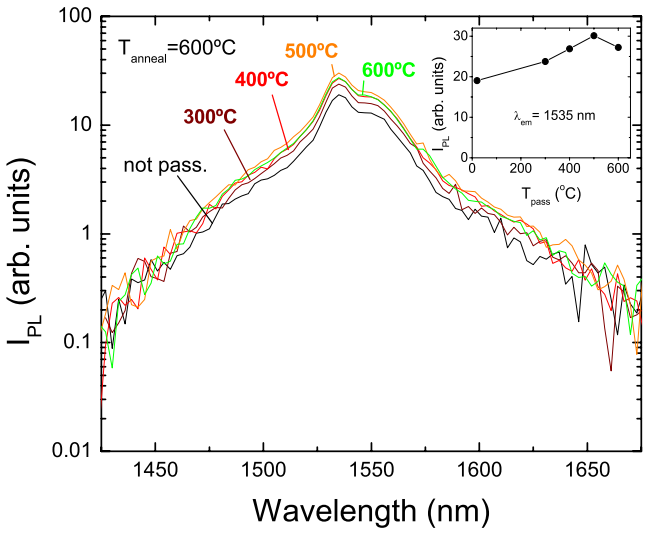

FIG. 2. (Color online) Photoluminescence spectra in the near-infrared region of LTA samples passivated in the temperature range of 300–600 °C. The PL spectrum of an unpassivated sample is included as a reference. Inset: PL intensity of the Er^{3+}-related emission of the LTA samples at 1535 nm as a function of passivation temperature.

and is ascribed to the emission from the luminescence centers in the Si-rich SiO_2 related to oxygen deficiencies.[1,39–42] Similar broad visible emission bands have been observed in Si-implanted thermally grown SiO_2 films,[29,30,39–41] as well as deposited Si-rich SiO_2 films[42] (present study), supporting the notion that stoichiometry rather than implantation damage is responsible for the formation of the luminescent centers. The photoluminescence peak at 981 nm is related to the optical transition of Er^{3+} ions from the second excited state ($^4I_{11/2}$) to the ground state ($^4I_{15/2}$). The spectral shape of the LC emission shows very little change as a function of passivation temperature. The emission at a wavelength of 750 nm was chosen to represent the LC intensity and is shown in the inset of Fig. 1. Passivation at temperatures up to 600 °C is seen to result in a gradual increase in the LC emission intensity by up to a factor of ~1.4 as compared to the unpassivated sample. It is worth mentioning that this increase in the LC-related emission upon passivation is different from observations on Si-implanted SiO_2 films,[30] wherein a *decrease* in a similar broad emission feature was observed upon passivation using deuterium implantation and subsequent annealing. This difference is not well understood, but it may be related to the different sample preparation and passivation methods used.

Figure 2 shows the photoluminescence spectra of the LTA samples in the near-infrared region. The observed emission band peaking at 1535 nm corresponds to the transition of Er^{3+} ions from their first excited state ($^4I_{13/2}$) to the ground state ($^4I_{15/2}$). The inset of Fig. 2 displays the PL intensity at 1535 nm as a function of passivation temperature. Similar to the moderate intensity increase in the LC-related emission (see inset of Fig. 1), an increase of up to a factor ~1.6 in the Er-related emission intensity at 1535 nm is observed with increasing passivation temperature.

Figure 3 shows the PL spectra in the visible–near-infrared region of the HTA samples passivated at temperatures in the range of 300–800 °C. The PL spectrum of the unpassivated sample is included for comparison. Again, a broad emission band is observed, in this case peaking at around 750–800 nm. This band is characterized by a relatively long decay time (τ=13–36 μs at λ=900 nm) and is attributed to radiative exciton recombination in silicon NCs.[43–46] The inset of Fig. 3 shows the behavior of the NC-related signal at 900 nm for different passivation temperatures. This wavelength was chosen in the present analysis to minimize the influence of nanocrystal-to-nanocrystal energy transfer on the photoluminescence properties. The probability of energy transfer is known to be lower for nanocrystals emitting at long wavelengths.[47,48] The nanocrystal-related emission intensity exhibits a significant increase upon passivation (up to a factor of ~40 at a wavelength of 900 nm). Contrary to the case of LTA samples, no Er^{3+}-related emission is observed at 981 nm. It should be noted that passivation leads to a significant change in the spectral shape of the NC emission: a higher passivation temperature leads to a relatively large increase in the long-wavelength PL intensity as compared to the increase observed at shorter wavelengths. Figure 4 shows the emission spectra of the HTA samples in the near-infrared region. Similar to the case of LTA, a clear Er^{3+} emission spectrum is observed peaking at 1535 nm. The dependence of the Er^{3+} PL intensity at 1535 nm on passivation temperature is shown in the inset of Fig. 4. A significant increase in the Er-related emission intensity of up to a factor ~9 is observed upon passivation.

Figure 5(a) shows the measured PL lifetime of the Er^{3+} emission at 1535 nm ($\tau_{dec,Er}$) as a function of passivation temperature of the LTA samples (closed circles) and the HTA samples (open circles). Error bars are included for data sets with a relative error in excess of 5%. Note that all panels in Fig. 5 display the same dynamic range (3 orders of magnitude) to facilitate comparison of the relative changes in each

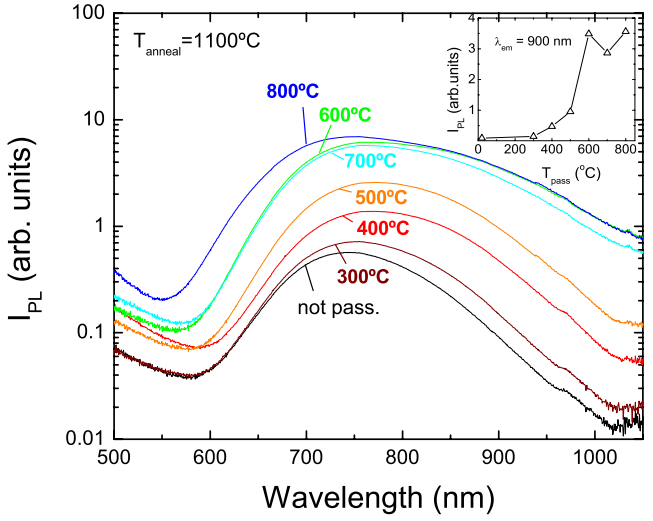

FIG. 3. (Color online) Photoluminescence spectra in the visible–near-infrared region of the HTA samples passivated in the temperature range of 300–800 °C. The PL spectrum of an unpassivated sample is included as a reference. Inset: PL intensity of nanocrystal-related emission of the HTA samples at 900 nm as a function of passivation temperature.

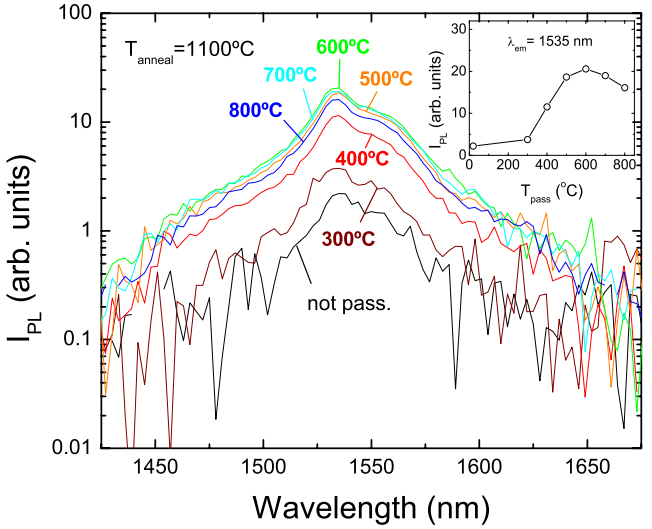

FIG. 4. (Color online) Photoluminescence spectra in the near-infrared region of the HTA samples passivated in the temperature range of 300–800 °C. The PL spectrum of an unpassivated sample is included as a reference. Inset: PL intensity of Er^{3+}-related emission of the HTA samples at 1535 nm as a function of passivation temperature.

of the measured parameters. All Er^{3+} decay traces were found to exhibit a degree of multiexponentiality and could be accurately described by the Kohlrausch–Williams–Watts function $I(t) \propto \exp[-(t/\tau_{dec})^{\beta}]$ with a dispersion factor β in the range of 0.75–0.82. The Er^{3+} lifetimes are seen to remain relatively constant as a function of passivation temperature in both sample types and are on the order of ~50 μs and ~450 μs in the LTA and HTA samples, respectively. The longer Er^{3+} lifetime after high-temperature annealing is commonly attributed to the thermally activated removal of nonradiative recombination centers in the oxide matrix directly affecting the Er^{3+} decay rate.[49,50]

The nanocrystal PL decay times in the HTA samples ($\tau_{dec,NC}^{HTA}$) measured at 800 nm and at 900 nm are included in Fig. 5(a) (open squares and open triangles, respectively). Similar to the Er^{3+} PL decay traces, the nanocrystal PL decay traces also exhibit a multiexponential behavior with a dispersion factor in the range of 0.60–0.76. A gradual increase in the nanocrystal lifetime with increasing passivation temperature is observed at both detection wavelengths. The lifetimes of the luminescence-center-related band measured at 550 nm are not included in Fig. 5 since they were found to be shorter than the time resolution of 80 ns.

Figure 5(b) shows the effective absorption cross section σ_{abs} for Er^{3+} excitation in the LTA (closed circles) and HTA samples (open circles) as found based on the measured excitation rate R_{exc} using the well known relation

$$R_{exc} = \sigma_{abs}\phi = \frac{1}{\tau_{rise}} - \frac{1}{\tau_{dec}}, \quad (1)$$

where φ is the known incident pump photon flux and τ_{rise} and τ_{dec} are the experimentally determined rise and decay times, respectively. The measured Er^{3+} and nanocrystal rise times (not shown) exhibit a similar dependence on passivation temperature as the corresponding decay times. The effective Er^{3+} excitation cross sections are found to be similar in magnitude for both sample types and are relatively independent of the passivation temperature, varying by a factor of ~2 across the entire temperature range. The effective Er^{3+} absorption cross sections are found to be $(0.7–1.6) \times 10^{-15}$ cm^2 in the LTA samples and $(2.3–4.2) \times 10^{-15}$ cm^2 in the HTA samples. Note that the values reported here for the HTA sample are a factor of ~6 lower than the values reported in Ref. 1 due to a more accurate determination of the laser spot size in the present study. Additionally, in Ref. 1 the Er^{3+} excitation cross section in the LTA samples was found to be approximately equal to that in the HTA sample, whereas in the present study the effective Er^{3+} absorption cross section observed in the LTA samples is found to be a factor of ~2–3 lower as compared to that in the HTA samples. The reason of this discrepancy is not known, but it may be caused by a small degree of sample aging, particularly for samples annealed at low temperatures.

The effective nanocrystal absorption cross section in the HTA samples was also determined as a function of passivation temperature using Eq. (1), based on the $1/e$ rise times and decay times measured at a wavelength of 900 nm. The corresponding cross-section values are included in Fig. 5(b) (open triangles) and are found to be relatively independent of passivation temperature. The measured NC cross section of $\sigma_{NC} \approx 1 \times 10^{-14}$ cm^2 under 351 nm excitation is in good agreement with known literature values.[51]

The relatively small variation in the measured lifetimes in Fig. 5(a) and the absorption cross sections in Fig. 5(b) suggests that most of the observed changes in the Er^{3+} and nanocrystal PL intensity are related to the number of contributing emitters. In order to verify this, the concentration of optically active Si nanocrystals as well as the concentration of sensitized optically active Er^{3+} ions were determined as a function

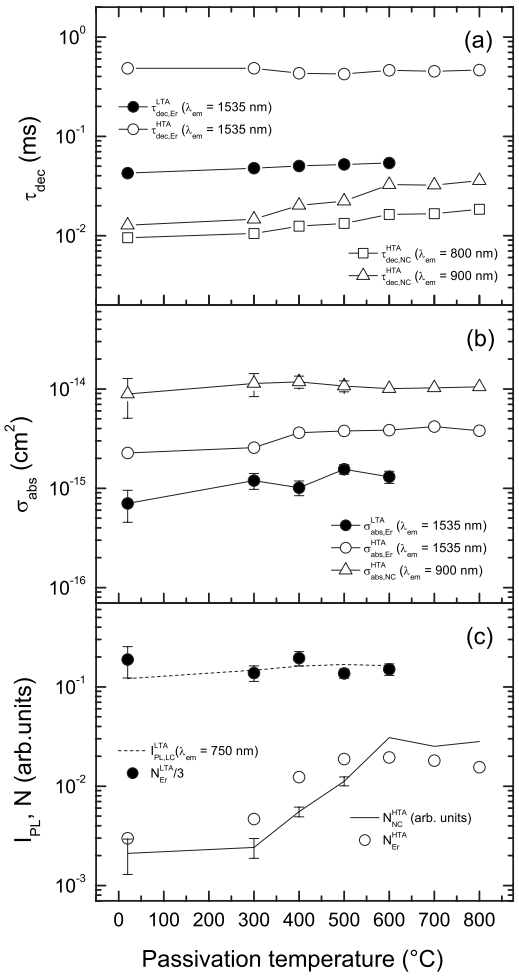

FIG. 5. Measured and deduced photoluminescence parameters of the LTA (solid symbols) and HTA samples (open symbols) as a function of passivation temperature: (a) Er^{3+} PL decay times at 1535 nm of the LTA and HTA samples ($\tau^{LTA}_{dec,Er}$ and $\tau^{HTA}_{dec,Er}$, respectively) and silicon nanocrystal PL decay times at 800 and 900 nm in the HTA samples ($\tau^{HTA}_{dec,NC}$); (b) the effective absorption cross sections of the Er^{3+} PL at 1535 nm in the LTA and HTA samples ($\sigma^{LTA}_{abs,Er}$ and $\sigma^{HTA}_{abs,Er}$ respectively), and of the silicon nanocrystal PL at 900 nm in the HTA samples ($\sigma^{HTA}_{abs,NC}$); (c) luminescence center PL intensity at 750 nm in the LTA samples ($I^{LTA}_{PL,LC}$), the relative density of sensitized optically active Er^{3+} ions in the LTA and HTA samples (N^{LTA}_{Er} and N^{HTA}_{Er}, respectively), and the relative density of optically active silicon nanocrystals contributing to the emission at 900 nm (N^{HTA}_{NC}). The arbitrary units of the relative density of sensitized optically active Er^{3+} ions and optically active silicon nanocrystals are not related.

of passivation temperature. In the case of finite signal saturation and for a fixed film thickness and excitation and collection geometry, the PL intensity I_{PL} depends on the density of active emitters, N, according to

$$I_{PL} \propto \frac{R_{exc}\tau_{dec}}{1 + R_{exc}\tau_{dec}} N. \tag{2}$$

This equation relies on the common assumption that the Er^{3+} ions and the Si nanocrystals can be modeled as a quasi-three-level system. The concentration of emitters is thus proportional to

$$N \propto \left(1 + \frac{1}{R_{exc}\tau_{dec}}\right) I_{PL}. \tag{3}$$

The term $R_{exc}\tau_{dec}$ is an indication of the excited state population of the emitter, with a value of 1 corresponding to the onset of population inversion. The magnitude of this term depends on the origin of the photoluminescence and on the measurement conditions, and in these studies is ~0.02–0.03 in the Er^{3+} PL measurements on the LTA samples, ~0.06–0.19 in the NC PL measurements on the HTA samples, and ~0.54–0.93 in the Er^{3+} PL measurements on the HTA samples. Figure 5(c) shows the behavior of the density of sensitized optically active Er^{3+} ions obtained from Eq. (3) as a function of passivation temperature for the LTA (closed circles) and HTA samples (open circles), as well as the concentration of optically active nanocrystals (solid line) based on the measured PL intensities, cross sections, and lifetimes. For comparison, the luminescence center emission intensity observed in the LTA samples at 750 nm has been included (dashed line) in Fig. 5(c). For the LTA samples, a relatively constant density of sensitized optically active Er^{3+} ions is observed as the passivation temperature is increased up to 600 °C. Notably, relatively little change is observed in the LC PL intensity (measured at λ_{em}=750 nm) in this same passivation temperature range. In contrast, for the HTA samples an increase in the density of sensitized optically active Er^{3+} ions and of optically active Si nanocrystals contributing to the emission at λ_{em}=900 nm by factors of ~6.5 and ~14.6, respectively, is observed in the same temperature range. Note that the exact change in the density of optically active Si nanocrystals most likely depends on the nanocrystal size and therefore on the emission wavelength. However, from the spectra shown in Fig. 3, it is clear that a significant increase in nanocrystal emission occurs for all wavelengths shown.

The observations made above appear to challenge several existing theories. First, in our previous work[1] we demonstrated that LCs are responsible for the majority of Er^{3+} excitation events for all annealing temperatures up to 1200 °C, whereas the present data show a clear correlation between the Si nanocrystal PL intensity and the Er^{3+} PL intensity. Second, the observation of a gradual improvement of the NC lifetime upon passivation appears to contradict the existing theory that hydrogen passivates surface traps at the Si-SiO_2 interface, activating previously entirely "dark" nanocrystals.[27] This kind of "dark"/"bright" classification would predict a nanocrystal lifetime that is independent of the passivation temperature, rather than the experimentally observed gradual increase in the NC decay time with increasing passivation temperature. Both these apparent contradictions can be resolved, as discussed below.

B. Discussion

1. Effect of passivation on Er^{3+} *excitation*

Based on the experimental results presented here, as well as those present in the literature, a model is needed that can

simultaneously account for all of the following observations:

(i) The similarity between the LC excitation spectrum and the Er^{3+} excitation spectrum.[1]

(ii) The correlation between the Er^{3+} excitation density and the LC emission intensity as a function of *annealing* temperature up to 1000 °C.[1]

(iii) The similarity between the measured effective absorption cross sections for Er^{3+} excitation in samples with and without Si nanocrystals[1] (present study).

(iv) The relative insensitivity of the effective Er^{3+} absorption cross section to the Er concentration.[16]

(v) The presence of fast and slow Er^{3+} excitation mechanisms.[22,24]

(vi) The decrease in the NC lifetime upon Er^{3+} incorporation.[1,65]

(vii) The correlation between the density of sensitized optically active Er^{3+} ions and the LC emission intensity as a function of *passivation* temperature in samples without Si nanocrystals (present study).

(viii) The correlation between the density of sensitized optically active Er^{3+} ions and the density of optically active Si nanocrystals as a function of passivation temperature in samples containing Si nanocrystals (present study).

(ix) The larger sensitivity of the Er^{3+} PL to passivation in samples containing nanocrystals as compared to samples wherein no nanocrystals are present (present study).

(x) The increase in the Er-related emission intensity at lower passivation temperatures as compared with the NC-related emission intensity[25] (present study).

(xi) The significant reduction in the NC PL intensity[1,12,16,21,52] and the LC PL intensity[1] as a result of Er incorporation.

(xii) The absence of resonance features in the NC emission spectrum in Er-doped samples at wavelengths corresponding to optical transitions of Er^{3+}.[1,12,52,53]

(xiii) The similarity between the magnitudes of the measured Si nanocrystal absorption cross section and of the effective Er^{3+} absorption cross section in samples containing Si nanocrystals[1,16,17,47] (present study).

(xiv) The similarity between the LC excitation spectrum and the NC excitation spectrum.[1]

In our previous work,[1] based on observations (i)–(iii) we concluded that the Er^{3+} excitation in these silicon-doped SiO_2 samples occurs predominantly through a luminescence-center-mediated process, while a small fraction of the excitation events occurs via Si nanocrystals. This interpretation also accounts for observations (iv)–(vi) and is further supported by our observation in the present study showing that passivation affects the LC PL intensity and the density of sensitized optically active Er^{3+} ions in the same way [observation (vii)]. Despite this correspondence, a number of observations are present that appear to contradict the model proposed in the previous study. First of all, the correlation between the density of sensitized optically active Er^{3+} ions and the density of optically active Si nanocrystals as a function of passivation temperature [observation (viii)] suggests that the presence of nanocrystals can significantly affect the Er^{3+} photoluminescence. The influence of nanocrystals on the Er^{3+} PL is further confirmed by the fact that the Er^{3+} PL intensity and the density of sensitized optically active Er^{3+} ions are found to be sensitive to passivation only when nanocrystals are present [observation (ix)]. This leaves us with a paradox: while annealing studies[1] strongly suggest that nanocrystals are not required for Er^{3+} excitation, our passivation studies show that their presence can strongly influence the optical properties of the Er^{3+} ions.

To resolve this paradox, the excitation model presented in our previous studies[1] needs to be extended without introducing any conflicts with earlier observations. We first consider the effect of passivation on the nanocrystal PL intensity. Electron paramagnetic resonance (EPR) studies on Si-rich SiO_2 samples have shown that P_b-type defects (silicon dangling bonds) form predominantly at the Si-SiO_2 interface due to a lattice mismatch between the Si nanocrystals and the amorphous SiO_2 matrix.[35,36] The experimentally observed anticorrelation of the NC PL intensity and the density of P_b-type defects measured by EPR as a function of passivation temperature[25] and of the passivation time[54] has demonstrated that the presence of silicon dangling bonds results in a reduced nanocrystal PL intensity. We therefore conclude that the observed nanocrystal PL increase seen in Fig. 3 is due to the saturation of silicon dangling bonds with hydrogen upon passivation at elevated temperatures. Second, we consider the behavior of the Er^{3+} PL intensity. From Fig. 5(c) we see that the dependence of the concentration of indirectly excitable and optically active Er^{3+} ions on passivation is similar to that of the concentration of optically active Si nanocrystals. Since we have previously demonstrated that LC-mediated Er^{3+} excitation is the dominant Er^{3+} excitation mechanism in these samples,[1] we must conclude that the observed improvement of the Er^{3+} PL intensity upon passivation *cannot be related to a change in a nanocrystal-mediated excitation process*. Instead, we propose that the presence of unpassivated nanocrystals leads to either suppression of the LC-mediated Er^{3+} excitation process or to the introduction of a nonradiative Er^{3+} relaxation process in HTA samples. Based on the relatively long lifetimes of the Er^{3+} excited states, the latter possibility appears the most likely. Since no significant passivation-dependent changes were observed in the Er^{3+} decay traces at 1.5 μm of the HTA samples, it appears that this nonradiative interaction does not involve the Er^{3+} first excited state. We therefore propose that the presence of silicon dangling bonds at the nanocrystal surface can introduce a rapid nonradiative Er^{3+} relaxation from one or more of the Er^{3+} energy levels above the first excited state to the ground state. In this way, dangling bonds could reduce the excitation efficiency of the Er^{3+} first excited state, leading to the experimentally observed lower Er^{3+} emission intensity. Based on our experimental observations, we propose that the presence of a dangling bond enables an Auger process in which nonradiative Er^{3+} relaxation is accompanied by the promotion of an electron from a neutral P_b center to the quantum confined conduction band of a Si nanocrystal. Based on the known location of the neutral dangling bond state relative to the silicon valence band ($\sim$0.3 eV above the valence band of bulk silicon),[55,56] it is expected that this process would require 0.8 eV in unconfined silicon systems with a band gap of 1.1 eV and more in quantum confined systems due to the additional confinement energy that would need to be overcome. Based on the

known emission energies of 0.8, 1.3, and 1.5 eV of the first, second, and third excited states of Er^{3+}, respectively, it indeed is physically reasonable to assume that the first excited state would not have a sufficient energy to induce such an Auger process in our nanocrystal-doped samples, which fits with our experimental observations. Note that this process would also result in a lower apparent Er^{3+} excitation rate at low passivation temperatures since the LC-mediated excitation into higher lying states would have a reduced probability of bringing Er^{3+} into the first excited state. A reduced Er^{3+} excitation rate is indeed observed in Fig. 5(b) for the unpassivated HTA sample and for the HTA sample passivated at 300 °C.

With the model proposed above, we can now understand the passivation temperature dependence of the photoluminescence properties of the HTA samples in Fig. 5(c). As the passivation temperature is increased, the average number of silicon dangling bonds on Si nanocrystals is reduced and the number of fully passivated nanocrystals increases. This leads to a simultaneous increase in the nanocrystal and Er^{3+} PL intensity: the nanocrystal PL increases due to an increased density of fully passivated optically active nanocrystals, while the Er^{3+} PL increases due to a reduced nonradiative coupling of the Er^{3+} ions to silicon dangling bonds.

Using the data in Fig. 5(c), we can estimate the fraction of sensitized optically active Er^{3+} ions in the HTA samples that is affected by the presence of silicon dangling bonds. As was shown before, the density of sensitized optically active Er^{3+} ions in HTA samples increased by a factor of ~6.5 upon passivation. This implies that before passivation, a large fraction of the indirectly excitable Er^{3+} ions was affected by the presence of unpassivated nanocrystals. We can determine an upper bound on the fraction of affected Er^{3+} ions by noting that the fully passivated sample contains at most 100% active Er^{3+} ions. This implies that at most 100%/6.5=15% of the Er^{3+} ions were unaffected by the presence of unpassivated nanocrystals or, conversely, that at least 85% of the indirectly excitable Er^{3+} ions were affected by the presence of unpassivated nanocrystals. A consequence of this model is thus that a large fraction of the Er^{3+} ions is in close proximity to at least one silicon dangling bond in unpassivated samples. This can be considered as a viable scenario given the high Si concentration in the samples under study.

The experimental results presented in Fig. 5(c) seem to indicate that the density of sensitized optically active Er^{3+} ions in the HTA samples stabilizes at a passivation temperature of 500 °C, while the density of optically active nanocrystals stabilizes at a passivation temperature of 600 °C. This was also observed by Fukata *et al.*[25] in combined PL and EPR studies but as a function of hydrogen diffusion. A possible physical origin for these observations is schematically shown in Fig. 6. At low passivation temperatures [Fig. 6(a)], Si nanocrystals (large circles in Fig. 6) may contain multiple dangling bonds, as indicated by the crosses at the Si-SiO_2 interface, rendering the nanocrystals "dark". In our model, these dangling bonds can affect the Er^{3+} ions within a certain interaction range, as indicated by the dashed circles around the dangling bonds. The Er^{3+} ions are known to be located inside the silica matrix[57] or at the nanocrystal-silica interface,[57,58] as shown schematically in Fig. 6. At low passivation temperatures, a large fraction of the Er^{3+} ions is affected by the dangling bonds, as indicated by the dark small circles; while a small fraction of the Er^{3+} ions is unaffected, as indicated by the small open circles. As the passivation temperature is increased [Fig. 6(b)], the dangling bonds become hydrogen passivated, as indicated by the letter H in Fig. 6. This leads to a decrease in the number of affected Er^{3+} ions and a corresponding increase in the Er^{3+} emission intensity. Importantly, at this same passivation temperature, the nanocrystal emission intensity does not show a similar increase since the presence of a single dangling bond can render a nanocrystal optically "dark". Only at higher passivation temperatures does the number of nanocrystals that are fully passivated increase significantly, as indicated by the light-colored circles in Fig. 6(c), resulting in the observed increase in the nanocrystal emission intensity.

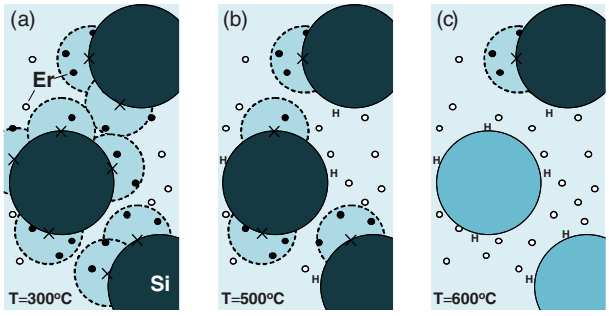

FIG. 6. (Color online) Proposed model of the effect of hydrogen passivation on the Si nanocrystal and Er^{3+} emission at three different passivation temperatures: (a) 300, (b) 500, and (c) 600 °C. The large dark and bright solid circles represent Si nanocrystals with low and high emission efficiencies, respectively. The crosses represent dangling bonds, the dashed circles schematically indicate the interaction range of a dangling bond, and the letter H represents a hydrogen terminated dangling bond. The small solid and open circles represent Er^{3+} ions that are affected or unaffected by a dangling bond, respectively.

The argument that dangling bonds affect the Er^{3+} ions directly also explains the observed weak sensitivity to passivation of the Er^{3+} and LC PL in the LTA samples. According to published EPR studies, no P_b centers are present in unannealed Si-rich SiO_2 samples[59] and dangling bonds are formed only at crystalline silicon–SiO_2 interfaces[35,36] with their concentration increasing in the process of nanocrystal formation.[60] Taking into account that no crystalline phase has been observed in LTA samples,[1] dangling bonds are expected to be absent in these samples. As a result, passivation only has a minor effect on the Er^{3+} emission as well as on the LC emission efficiency in samples where no nanocrystals are present.

The arguments given above provide an explanation for observations (vii)–(x), and since our model maintains the LC-mediated nature of the Er^{3+} excitation, observations (i)–(vi) are still in agreement with this model. Intriguingly, the remaining unexplained observations (xi)–(xiv) can all be accounted for by assuming that luminescence centers not only can excite Er^{3+} ions but also can generate excitons in Si nanocrystals. If we consider LCs to be an important source of nanocrystal excitation, then addition of Er^{3+} could lead to

a reduced probability of nanocrystal excitation, resulting in a reduced nanocrystal emission intensity, as commonly observed in literature,[1,12,16,21,52] but without introducing any resonance features in the nanocrystal emission spectrum associated with NC→Er^{3+} excitation. The absence of such resonance features was reported in numerous PL studies on Er-doped Si-rich SiO_2.[1,12,52,53] This would also naturally explain the similar values of the typical nanocrystal absorption cross section and of the effective Er^{3+} absorption cross section,[1,13] as well as the good correspondence between the LC and NC excitation spectra.[1]

2. Effect of passivation on the nanocrystal lifetimes

Figure 5(a) shows that the nanocrystal emission lifetimes at 800 and at 900 nm both increase gradually as the passivation temperature is increased. This is a surprising result that cannot readily be understood in terms of passivation-induced changes in the emission lifetime of individual nanocrystals. To clarify this statement, we consider the possible exciton decay channels. The total exciton lifetime is governed by (a) radiative exciton recombination,[61] (b) nonradiative exciton trapping by silicon dangling bonds,[27,31,32] (c) energy transfer to a nearby nanocrystal,[62–64] and (d) energy transfer to a nearby Er^{3+} ion.[1,22,65] The total decay rate of excitons in nanocrystals of a specific size is therefore given by

$$R_{\mathrm{dec,NC}} = R_{\mathrm{rad,NC}} + N_{\mathrm{DB}} \times R_{\mathrm{DB}} + R_{\mathrm{NC\text{-}NC,tot}} + R_{\mathrm{NC\text{-}Er,tot}},$$

where $R_{\mathrm{rad,NC}}$ is the exciton radiative decay rate, R_{DB} is the exciton capture rate by a single silicon dangling bond, N_{DB} is the number of silicon dangling bonds per nanocrystal, $R_{\mathrm{NC\text{-}NC,tot}}$ is the total energy transfer rate to nearby larger nanocrystals, and $R_{\mathrm{NC\text{-}Er,tot}}$ is the total energy transfer rate from the nanocrystal to nearby Er^{3+} ions. These rates affect the nanocrystal emission efficiency given by $\eta_{\mathrm{NC}} = R_{\mathrm{rad,NC}}/R_{\mathrm{dec,NC}}$. Of all the decay contributions, the number of silicon dangling bonds is expected to depend most strongly on the passivation treatment. The other three contributions ($R_{\mathrm{rad,NC}}$, $R_{\mathrm{NC\text{-}NC,tot}}$, and $R_{\mathrm{NC\text{-}Er,tot}}$) are thought to depend on, respectively, the nanocrystal size and shape, the nanocrystal density, and the Er^{3+} distribution, none of which are expected to change significantly for passivation temperatures well below the annealing temperature used.

Based on theoretical works,[31,32] the exciton capture rate of a silicon dangling bond at the Si-SiO_2 interface was calculated to be $\sim 10^{10}$–10^{11} s^{-1} for nanocrystals with peak PL intensities at ~750 nm. By comparison, the other possible decay channels are dramatically slower. The typical room temperature radiative decay rate of excitons in nanocrystals emitting at these wavelengths is $R_{\mathrm{rad,NC}} \sim 10^3$–$10^4$ s^{-1} (Refs. 61 and 65) while the experimentally observed nanocrystal-to-erbium energy transfer rate constant is $\sim 10^4$–10^6 s^{-1}.[1,22,65] This suggests that the presence of a single silicon dangling bond ($N_{\mathrm{DB}}=1$) can reduce the nanocrystal emission efficiency by several orders of magnitude, rendering the nanocrystals effectively "dark", i.e., virtually undetectable in photoluminescence spectra and in lifetime measurements. We thus expect Si-nanocrystal-doped samples to contain (a) *unpassivated nanocrystals with one or more silicon dangling bonds* that are optically undetectable due to an extremely low emission efficiency given by

$$\eta_{\mathrm{NC,unpass}} = \frac{R_{\mathrm{rad,NC}}}{R_{\mathrm{rad,NC}} + N_{DB} \times R_{DB} + R_{\mathrm{NC\text{-}NC,tot}} + R_{\mathrm{NC\text{-}Er,tot}}} \approx 0,$$

as well as (b) *fully passivated nanocrystals that do not have a silicon dangling bond* and have a relatively high emission efficiency given by

$$\eta_{\mathrm{NC,pass}} = \frac{R_{\mathrm{rad,NC}}}{R_{\mathrm{rad,NC}} + R_{\mathrm{NC\text{-}NC,tot}} + R_{\mathrm{NC\text{-}Er,tot}}}.$$

These arguments suggest that the total nanocrystal photoluminescence intensity and the measured decay rate will reflect only the lifetime of fully passivated nanocrystals. Consequently, the measured nanocrystal lifetime is expected to be independent of the passivation temperature. This is in clear contradiction with the observations in Fig. 5(a).

To resolve the apparent contradiction described above, we consider the inhomogeneous nature of the nanocrystal emission spectrum. As was observed in Fig. 5(a), the nanocrystal lifetime at an emission wavelength of 800 nm is found to be a factor of 1.3–2 shorter than that observed at 900 nm. Such a wavelength-dependent emission lifetime has been attributed to two different phenomena: (i) the size-dependent oscillator strength of the transitions in the nanocrystals, resulting in the size-dependent radiative decay rates of the nanocrystals;[66,67] and (ii) the presence of energy transfer from small nanocrystals that have a large band gap to larger nanocrystals that have a smaller band gap.[47,48,62–64] Both these effects lead to a shorter lifetime for smaller nanocrystals emitting at shorter wavelengths. As will be shown below, this size-dependent emission lifetime can lead to an *apparent* gradual change in the nanocrystal lifetime at a single emission wavelength due to the inhomogeneous nature of the nanocrystal emission spectrum. The nanocrystal emission spectra in this type of sample are well known to be inhomogeneously broadened, with the short-wavelength emission being largely due to emission by small (rapidly decaying) nanocrystals and the long wavelength emission originating predominantly from large (slowly decaying) nanocrystals. As demonstrated in Ref. 68, the homogeneous emission linewidth of a silicon nanocrystal with a diameter of ~3–4 nm is ~120 meV (~50 nm) at a peak emission energy of ~1.7 eV (~730 nm) as compared to the observed spectral width of ~350–500 meV (~160–230 nm) of the nanocrystal-related emission band peaking at ~1.66 eV (~750 nm) in the current study. The significant inhomogeneous broadening enables the observation of different lifetimes in different parts of the spectrum. More importantly, the nanocrystal emission detected at a wavelength of 900 nm contains a significant PL contribution from nanocrystals that exhibit a slightly different peak emission wavelength and that have a different lifetime. A gradual change in the apparent emission lifetime may thus be expected at a specific emission wavelength if the *relative photoluminescence contribution of nanocrystals with different sizes changes as a function of passivation temperature*. This effect is illustrated in Fig. 7 using the measured emission spectra. The left inset shows the measured NC emission spectrum (thick solid line)

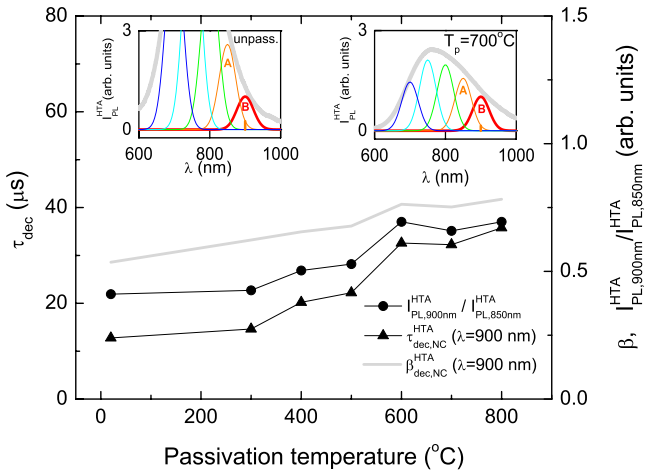

FIG. 7. (Color online) Measured and deduced photoluminescence parameters of the silicon-nanocrystal-related emission in the HTA samples as a function of passivation temperature: the ratio of the silicon nanocrystal PL intensity at 900 nm to that at 850 nm ($I^{\mathrm{HTA}}_{\mathrm{PL,900\ nm}}/I^{\mathrm{HTA}}_{\mathrm{PL,850\ nm}}$), silicon nanocrystal PL decay times of the HTA samples at 900 nm ($\tau^{\mathrm{HTA}}_{\mathrm{dec,NC}}$), silicon nanocrystal PL decay time dispersion factor of the HTA samples at 900 nm ($\beta^{\mathrm{HTA}}_{\mathrm{dec,NC}}$). Insets: Measured silicon nanocrystal emission spectra (thick solid line) for an unpassivated HTA sample (left) and for a HTA sample passivated at 700 °C (right), normalized at a wavelength of 900 nm. The Gaussian curves underneath the PL spectrum schematically depict the individual PL contributions of silicon nanocrystals with different sizes.

for an unpassivated HTA sample, normalized at a wavelength of 900 nm. The Gaussian curves underneath the PL spectrum schematically depict the individual PL contributions of nanocrystals with different sizes. The linewidth of all Gaussian curves was chosen to be equal to the known homogeneous linewidth[68] of ~120 meV. Note that emission by nanocrystals with a center wavelength of 850 nm (curve A) leads to a finite contribution to the PL intensity observed at 900 nm (curve B). This PL contribution, indicated by the short vertical line, will lead to the addition of a small fast lifetime component in PL decay traces recorded at 900 nm. Experimentally, this appears as a relatively short lifetime at $\lambda_{\mathrm{em}}=900$ nm and a low β value due to the stronger deviation from single-exponential decay. Note that the relatively weak emission from nanocrystals with a peak emission wavelength of 950 nm also adds a small contribution to the PL detected at 900 nm. For simplicity, we do not consider this minor contribution here. The right inset of Fig. 7 shows the NC emission spectrum (thick solid line) for a HTA sample passivated at 700 °C. According to the model introduced above, passivation has lead to a change in the number of optically active nanocrystals emitting at various wavelengths, while their individual lifetimes are unchanged. Similar to what was observed in the left inset, nanocrystals with a peak emission wavelength of 850 nm add a finite PL contribution at a detection wavelength of 900 nm. However, due to the change in the shape of the NC emission spectrum, the *relative contribution of emission from these nanocrystals to the photoluminescence at 900 nm is reduced.* This reduction in the short-wavelength contribution, as well as the concurrent reduction in the short-lifetime contribution at 900 nm, leads to a longer $1/e$ lifetime at $\lambda_{\mathrm{em}}=900$ nm and an increased β value. Both of these effects are clearly observed experimentally. Note that the analysis above considered only two discrete peak emission wavelengths, while in reality the emission at 900 nm contains contributions from nanocrystals with a range of peak emission wavelengths near 900 nm that is given by the homogeneous linewidth.

To further verify the proposed role of inhomogeneous broadening on the measured nanocrystal decay traces, Fig. 7 includes the measured nanocrystal decay time at an emission wavelength of 900 nm (triangles), the corresponding dispersion factor $\beta^{\mathrm{HTA}}_{\mathrm{dec,NC}}$ (solid line), and the ratio of the nanocrystal-related photoluminescence intensity observed at 900 and at 850 nm (circles), labeled $I^{\mathrm{HTA}}_{\mathrm{PL,900\ nm}}/I^{\mathrm{HTA}}_{\mathrm{PL,850\ nm}}$. The experimental error is less than 5% in all these data sets and has not been included in the graph. The plotted intensity ratio is a measure of the relative contribution of short-wavelength emission (850 nm) to the PL detected at 900 nm. Excellent qualitative correspondence is observed between the measured nanocrystal decay time and the intensity ratio $I^{\mathrm{HTA}}_{\mathrm{PL,900\ nm}}/I^{\mathrm{HTA}}_{\mathrm{PL,850\ nm}}$, despite the very different natures of these quantities. Further support for this interpretation is provided by the behavior of the dispersion factor $\beta^{\mathrm{HTA}}_{\mathrm{dec,NC}}$. As the relative contribution of the emission peaking at 850 nm to the PL intensity at 900 nm decreases, the dispersion factor is seen to gradually increase, which can be attributed to the reduced influence of smaller nanocrystals on the PL decay traces measured at 900 nm: as the relative PL contribution from smaller nanocrystals is reduced, fast lifetime components are being removed from the PL decay trace at 900 nm, leading to a more single-exponential decay and a β value closer to 1.

Based on the clear correlation of the shape of the photoluminescence spectra with the passivation-induced changes in the PL lifetime and in the measured β values, we conclude that the gradual nanocrystal lifetime increase observed upon passivation is *not* due to a gradual improvement of the nanocrystal emission efficiency, but it is rather a result of the inhomogeneous nature of the nanocrystal PL spectrum combined with a size-dependent degree of nanocrystal passivation at each temperature. This model also explains the relatively small increase in the NC lifetime with passivation temperature observed both in the current and independent studies[27] compared to the large changes in nanocrystal PL intensity. A final observation is that the change in the shape of the nanocrystal emission spectrum upon passivation (Fig. 3) implies that large nanocrystals responsible for the long-wavelength shoulder of the NC emission spectra require higher temperatures to become fully passivated as compared with temperatures required by smaller nanocrystals. This could be a reflection of the fact that large nanocrystals have a larger Si-SiO_2 interface area. This leads to a larger number of silicon dangling bonds for large nanocrystals[26,28,69] and may therefore require longer passivation times or higher passivation temperatures in order to reach full saturation of all dangling bonds.

The findings presented in this study are of significant importance for the realization of gain in Er-doped Si-rich SiO_2 waveguides. First, Er^{3+} in Si-rich SiO_2 films is excited pre-

dominantly via luminescence centers. This implies that one can obtain the large Er^{3+} excitation cross-section enhancements that have been observed in literature but without the need for silicon nanocrystals. This is an important result since Si nanocrystals are known[7,19] to induce a significant amount of confined-carrier absorption at 1.5 μm due to the presence of long-lived excitons in the nanocrystals during excitation. The ability to enhance the Er^{3+} excitation without introducing significant free carrier absorption would therefore be a major step forward in the development of silicon sensitized Er^{3+} gain media. Second, a low annealing temperature (600 °C) was found to lead to a higher concentration of indirectly excitable Er^{3+} as compared with that for a high annealing temperature (1100 °C). The observed higher concentration of sensitized optically active Er^{3+} ions in the samples annealed at low temperature (600 °C) implies a reduction in the concentration of optically active Er^{3+} ions that are not sensitized. This in turn reduces the degree of ground state absorption due to unsensitized Er^{3+} ions. Additionally, due to the direct relation between optical gain and the density of excited emitters, the larger concentration of sensitized optically active Er^{3+} ions observed in the LTA samples implies that a higher gain can be achieved in LTA samples as compared with HTA samples. Third, it was found that dangling bonds at the Si-SiO_2 interface can efficiently quench the Er^{3+} PL. This implies that any nanocrystals present in the matrix need to be fully passivated in order to obtain maximum gain. All these observations indicate that annealing temperatures below the onset of nanocrystal formation are preferred in order to achieve maximum gain. It should be noted that the Er^{3+} lifetime in samples annealed at low temperature is significantly shorter than that observed in samples annealed at high temperatures. Although this would lead to higher required pump powers for population inversion, this drawback may be outweighed by the significant advantages of purely luminescence-center-mediated Er^{3+} excitation.

IV. CONCLUSION

The effect of hydrogen passivation at different temperatures on the luminescence-center-mediated sensitization of Er^{3+} has been studied in Er-doped Si-rich SiO_2 films containing no detectable Si nanocrystals (annealed at 600 °C) and containing Si nanocrystals (annealed at 1100 °C). Passivation is shown to have a minor effect on the photoluminescence properties of samples without nanocrystals, which is ascribed to the absence of dangling bonds in these samples. In contrast, samples containing silicon nanocrystals exhibit a significant increase in the density of optically active silicon nanocrystals upon passivation, which is accompanied by a gradual change in the nanocrystal lifetime and a significant increase in the density of sensitized optically active Er^{3+} ions. The observed concurrent increase in the densities of active silicon nanocrystals and sensitized optically active Er^{3+} ions is ascribed to a passivation-temperature-dependent concentration of dangling bonds, which influences the emission from Si nanocrystals and Er^{3+} ions in different ways. In the case of nanocrystal photoluminescence, the presence of a dangling bonds results in the rapid trapping of excitons followed by nonradiative decay. In the case of Er^{3+} photoluminescence, we conclude that an Er^{3+} ion excited via a luminescence center can relax nonradiatively via a direct interaction with dangling bonds present on the surface of nanocrystals. This interaction appears to predominantly affect excited states above the $^4I_{13/2}$ level and is accompanied by a reduced excitation rate of the $^4I_{13/2}$ level. In addition, the gradual increase in the lifetime of the nanocrystal-related photoluminescence is attributed to a passivation-induced change in the concentration of optically active nanocrystals with different sizes. This change, combined with the inhomogeneous nature of the nanocrystal emission spectrum in these samples, leads to a change in the measured nanocrystal photoluminescence decay time.

ACKNOWLEDGMENT

This work was supported by the National Science Foundation (CAREER No. ECCS-0644228).

*Corresponding author; osavchyn@mail.ucf.edu
†Also at Physics Department, University of Central Florida, 4000 Central Florida Blvd., Orlando, FL 32816, USA.
‡Also at School of Electrical Engineering and Computer Science, University of Central Florida, 4000 Central Florida Blvd., Orlando, FL 32816, USA.
§Also at Department of Mechanical, Materials and Aerospace Engineering, University of Central Florida, 4000 Central Florida Blvd., Orlando, FL 32816, USA.

[1] O. Savchyn, F. R. Ruhge, P. G. Kik, R. M. Todi, K. R. Coffey, H. Nukala, and H. Heinrich, Phys. Rev. B **76**, 195419 (2007).
[2] M. Lipson, J. Lightwave Technol. **23**, 4222 (2005).
[3] N. Daldosso, D. Navarro-Urrios, M. Melchiorri, C. García, P. Pellegrino, B. Garrido, C. Sada, G. Battaglin, F. Gourbilleau, R. Rizk, and L. Pavesi, IEEE J. Sel. Top. Quantum Electron. **12**, 1607 (2006).
[4] T. J. Kippenberg, J. Kalkman, A. Polman, and K. J. Vahala, Phys. Rev. A **74**, 051802(R) (2006).
[5] A. Polman, B. Min, J. Kalkman, T. J. Kippenberg, and K. J. Vahala, Appl. Phys. Lett. **84**, 1037 (2004).
[6] A. J. Kenyon, Semicond. Sci. Technol. **20**, R65 (2005).
[7] P. G. Kik and A. Polman, in *Proceedings of the NATO Advanced Research Workshop on Towards the First Silicon Laser*, Trento, Italy, 2002, edited by L. Pavesi, S. Gaponenko, and L. Dal Negro (Kluwer, Dordrecht, 2003), p. 383.
[8] A. Polman, D. C. Jacobson, D. J. Eaglesham, R. C. Kistler, and J. M. Poate, J. Appl. Phys. **70**, 3778 (1991).
[9] W. Miniscalco, J. Lightwave Technol. **9**, 234 (1991).
[10] A. Polman and F. C. J. M. van Veggel, J. Opt. Soc. Am. B **21**, 871 (2004).
[11] A. J. Kenyon, P. F. Trwoga, M. Federighi, and C. W. Pitt, J. Phys.: Condens. Matter **6**, L319 (1994).

[12] M. Fujii, M. Yoshida, Y. Kanzawa, S. Hayashi, and K. Yamamoto, Appl. Phys. Lett. **71**, 1198 (1997).
[13] P. G. Kik, M. L. Brongersma, and A. Polman, Appl. Phys. Lett. **76**, 2325 (2000).
[14] G. Franzò, V. Vinciguerra, and F. Priolo, Appl. Phys. A: Mater. Sci. Process. **69**, 3 (1999).
[15] F. Gourbilleau, M. Levalois, C. Dufour, J. Vicens, and R. Rizk, J. Appl. Phys. **95**, 3717 (2004).
[16] P. G. Kik and A. Polman, J. Appl. Phys. **88**, 1992 (2000).
[17] A. J. Kenyon, C. E. Chryssou, C. W. Pitt, T. Shimizu-Iwayama, D. E. Hole, N. Sharma, and C. J. Humphreys, J. Appl. Phys. **91**, 367 (2002).
[18] M. Wojdak, M. Klik, M. Forcales, O. B. Gusev, T. Gregorkiewicz, D. Pacifici, G. Franzò, F. Priolo, and F. Iacona, Phys. Rev. B **69**, 233315 (2004).
[19] A. Mimura, M. Fujii, S. Hayashi, D. Kovalev, and F. Koch, Phys. Rev. B **62**, 12625 (2000).
[20] P. G. Kik and A. Polman, J. Appl. Phys. **91**, 534 (2002).
[21] D. Pacifici, G. Franzò, F. Priolo, F. Iacona, and L. Dal Negro, Phys. Rev. B **67**, 245301 (2003).
[22] M. Fujii, K. Imakita, K. Watanabe, and S. Hayashi, J. Appl. Phys. **95**, 272 (2004).
[23] K. Imakita, M. Fujii, and S. Hayashi, Eur. Phys. J. D **34**, 161 (2005).
[24] I. Izeddin, A. S. Moskalenko, I. N. Yassievich, M. Fujii, and T. Gregorkiewicz, Phys. Rev. Lett. **97**, 207401 (2006).
[25] N. Fukata, C. Li, H. Morihiro, K. Murakami, M. Mitome, and Y. Bando, Appl. Phys. A: Mater. Sci. Process. **84**, 395 (2006).
[26] S. Cheylan and R. G. Elliman, Nucl. Instrum. Methods Phys. Res. B **175-177**, 422 (2001).
[27] A. R. Wilkinson and R. G. Elliman, Phys. Rev. B **68**, 155302 (2003).
[28] S. Cheylan and R. G. Elliman, Appl. Phys. Lett. **78**, 1225 (2001).
[29] S. P. Withrow, C. W. White, A. Meldrum, J. D. Budai, D. M. Hembree, Jr., and J. C. Barbour, J. Appl. Phys. **86**, 396 (1999).
[30] K. S. Min, K. V. Shcheglov, C. M. Yang, Harry A. Atwater, M. L. Brongersma, and A. Polman, Appl. Phys. Lett. **69**, 2033 (1996).
[31] M. Lannoo, C. Delerue, and G. Allan, J. Lumin. **70**, 170 (1996).
[32] C. Delerue, G. Allan, and M. Lannoo, Phys. Rev. B **48**, 11024 (1993).
[33] A. Stesmans, J. Appl. Phys. **92**, 1317 (2002).
[34] P. J. Caplan, E. H. Poindexter, B. E. Deal, and R. R. Razouk, J. Appl. Phys. **50**, 5847 (1979).
[35] Y. Nishi, Jpn. J. Appl. Phys. **10**, 52 (1971).
[36] P. M. Lenahan and J. F. Conley, Jr., J. Vac. Sci. Technol. B **16**, 2134 (1998).
[37] K. L. Brower, Phys. Rev. B **38**, 9657 (1988).
[38] http://www.genplot.com/
[39] T. Shimizu-Iwayama, K. Fujita, S. Nakao, K. Saitoh, T. Fujita, and N. Itoh, J. Appl. Phys. **75**, 7779 (1994).
[40] M. Ya. Valakh, V. A. Yukhimchuk V. Ya. Bratus', A. A. Konchits, P. L. F. Hemment, and T. Komoda, J. Appl. Phys. **85**, 168 (1999).
[41] J.-Y. Zhang, X.-M. Bao, N.-S. Li, and H.-Z. Song, J. Appl. Phys. **83**, 3609 (1998).
[42] A. J. Kenyon, P. F. Trwoga, C. W. Pitt, and G. Rehm, J. Appl. Phys. **79**, 9291 (1996).
[43] J. S. Biteen, N. S. Lewis, H. A. Atwater, and A. Polman, Appl. Phys. Lett. **84**, 5389 (2004).
[44] I. N. Yassievich and A. S. Moskalenko, Mater. Sci. Eng., B **105**, 192 (2003).
[45] M. V. Wolkin, J. Jorne, P. M. Fauchet, G. Allan, and C. Delerue, Phys. Rev. Lett. **82**, 197 (1999).
[46] M. L. Brongersma, P. G. Kik, A. Polman, K. S. Min, and H. A. Atwater, Appl. Phys. Lett. **76**, 351 (2000).
[47] F. Priolo, G. Franzò, D. Pacifici, V. Vinciguerra, F. Iacona, and A. Irrera, J. Appl. Phys. **89**, 264 (2001).
[48] A. Polman and R. G. Elliman, in *Proceedings of the NATO Advanced Research Workshop on Towards the First Silicon Laser*, Trento, Italy, 2002, edited by L. Pavesi, S. Gaponenko, and L. Dal Negro (Kluwer, Dordrecht, 2003), p. 209.
[49] A. Polman, D. C. Jacobson, A. Lidgard, J. M. Poate, and G. W. Arnold, Nucl. Instrum. Methods Phys. Res. B **59-60**, 1313 (1991).
[50] A. Polman, D. C. Jacobson, D. J. Eaglesham, R. C. Kistler, and J. M. Poate, J. Appl. Phys. **70**, 3778 (1991).
[51] D. Kovalev, J. Diener, H. Heckler, G. Polisski, N. Künzner, and F. Koch, Phys. Rev. B **61**, 4485 (2000).
[52] F. Priolo, G. Franzò, F. Iacona, D. Pacifici, and V. Vinciguerra, Mater. Sci. Eng., B **81**, 9 (2001).
[53] P. G. Kik and A. Polman, Mater. Sci. Eng., B **81**, 3 (2001).
[54] P. Pellegrino, B. Garrido, C. García, R. Ferré, J. A. Moreno, and J. R. Morante, Physica E (Amsterdam) **16**, 424 (2003).
[55] E. H. Poindexter, G. J. Gerardi, M.-E. Rueckel, P. J. Caplan, N. M. Johnson, and D. K. Biegelsen, J. Appl. Phys. **56**, 2844 (1984).
[56] N. M. Johnson, D. K. Biegelsen, M. D. Moyer, S. T. Chang, E. H. Poindexter, and P. J. Caplan, Appl. Phys. Lett. **43**, 563 (1983).
[57] G. Franzò, D. Pacifici, V. Vinciguerra, F. Priolo, and F. Iacona, Appl. Phys. Lett. **76**, 2167 (2000).
[58] X. L. Wu, Y. F. Mei, G. G. Siu, K. L. Wong, K. Moulding, M. J. Stokes, C. L. Fu, and X. M. Bao, Phys. Rev. Lett. **86**, 3000 (2001).
[59] M. López, B. Garrido, C. Bonafos, A. Pérez-Rodríguez, J. R. Morante, and A. Claverie, Nucl. Instrum. Methods Phys. Res. B **178**, 89 (2001).
[60] M. López, B. Garrido, C. García, P. Pellegrino, A. Pérez-Rodríguez, J. R. Morante, C. Bonafos, M. Carrada, and A. Claverie, Appl. Phys. Lett. **80**, 1637 (2002).
[61] M. S. Hybertsen, Phys. Rev. Lett. **72**, 1514 (1994).
[62] M. L. Brongersma, A. Polman, K. S. Min, E. Boer, T. Tambo, and H. A. Atwater, Appl. Phys. Lett. **72**, 2577 (1998).
[63] J. Linnros, N. Lalic, A. Galeckas, and V. Grivickas, J. Appl. Phys. **86**, 6128 (1999).
[64] L. Pavesi, J. Appl. Phys. **80**, 216 (1996).
[65] K. Watanabe, M. Fujii, and S. Hayashi, J. Appl. Phys. **90**, 4761 (2001).
[66] T. Takagahara and K. Takeda, Phys. Rev. B **46**, 15578 (1992).
[67] D. Kovalev, H. Heckler, G. Polisski, J. Diener, and F. Koch, Opt. Mater. **17**, 35 (2001).
[68] J. Valenta, R. Juhasz, and J. Linnros, Appl. Phys. Lett. **80**, 1070 (2002).
[69] D. Kovalev, H. Heckler, G. Polisski, and F. Koch, Phys. Status Solidi B **215**, 871 (1999).